Chemical Engineering Journal 162 (2010) 836–843

Contents lists available at ScienceDirect

Chemical Engineering Journal

journal homepage: www.elsevier.com/locate/cej

Synthesis and photocatalytic properties of nano-MoS_2/kaolin composite

Kun Hong Hu[a,b,*], Zhu Liu[a], Fei Huang[a], Xian Guo Hu[b], Cheng Liang Han[a]

[a] Department of Chemical and Materials Engineering, Hefei University, Hefei 230022, PR China
[b] Department of Environmental Protection and Monitoring, Hefei University of Technology, Hefei 230009, PR China

ARTICLE INFO

Article history:
Received 15 April 2010
Received in revised form 2 June 2010
Accepted 7 June 2010

Keywords:
Molybdenum disulfide
Kaolin
Nanoparticles
Catalytic degradation
Photocatalysis

ABSTRACT

A nano-MoS_2/kaolin composite was synthesized by calcining a MoS_3/kaolin precursor in H_2, which was obtained via a quick deposition of MoS_3 on kaolin under a strong acidic condition. The obtained nano-MoS_2/kaolin composite was characterized using X-ray diffraction spectroscopy, Brunauer–Emmett–Teller (BET) surface area, scanning electron microscopy, high-resolution transmission electron microscopy, thermal analysis, ultraviolet–visible spectroscopy, and Fourier transform infrared spectroscopy. The results show that the composite had a 16 m^2/g BET surface area. MoS_2 in the composite was composed of layered structures with thickness of ~5 nm and length of ~10 nm. The composite contained an intensive absorption at 380–500 nm, which is in the visible light region, and presented a positive catalytic effect on removing methyl orange from the aqueous solution. The catalytic activity of the composite was influenced by the initial concentration of methyl orange, the amount of the catalyst, the pH value, and the degradation temperature. In addition, the composite catalyst could be regenerated and repeatedly used via filtration. The deactivating catalyst could be reactivated after catalytic reaction by heating at 450 °C for 30 min in H_2. The kaolin can decrease the sizes of nano-MoS_2 and improve the photo absorption of the composite. Thus, the composite shows excellent catalytic properties. Moreover, the kaolin mineral is very cheap and the using of the composite is very low-cost and practical.

1. Introduction

The absorption edge of the titanium dioxide (TiO_2) falls in the UV region, which involves only ~3% of the sunlight spectrum. Thus, the application range of TiO_2-based photocatalysts is remarkably reduced. Fortunately, the photocatalytic activity of TiO_2 can be improved using nanosized TiO_2, mixing active additives to TiO_2, or performing advanced oxidation treatment [1–6]. Alternatively, to deal with such a problem, the photocatalytic capability of molybdenum disulfide (MoS_2) was also investigated as a possible solution [7,8].

MoS_2 with the typical layered structure and the weak van der Waals gap shows excellent properties such as catalysis, intercalation, lubrication, anisotropy, chemically inertness, photocorrosion resistance, and so on [9]. As for the catalytic properties, MoS_2 has been vastly used to remove S and N from crude oil [10–12]. Moreover, the energy gap of nanosized MoS_2 (nano-MoS_2) falls in the visible light region and leads to a potential application in photocatalysis [7,8,13–15]. The electronic states of the conduction and valence bands in layered bulk MoS_2 are both derived primarily from Mo 4d orbitals. Photoexcitation of electrons, therefore, should not significantly weaken Mo–S bonds, which is responsible for the remarkable photostability of bulk MoS_2 during photoelectrochemical oxidation of water [15,16]. When the size of MoS_2 is reduced to the nanoscale, such as in films and nanoclusters, Mo edge-site atoms are not protected by the inert basal planes of MoS_2. As a result, the band gap of nanoscale MoS_2 becomes small enough to allow most of the solar spectrum to be harvested. Meanwhile, nano-MoS_2 is relatively unstable in water, leading to the dissolution of the lattice via oxidation of sulfur to sulfate ions. However, this process is quite slow in a covalent material such as this, compared to ionic semiconductor electrodes such as CdS [17]. Thus, it is still possible for nano-MoS_2 to be employed for water treatment.

Nanosized MoS_2 (nano-MoS_2) has better properties than bulk MoS_2 and attracts considerable attention. Consequentially, some chemical routes to synthesize nanosized MoS_2 particles were reported [18–26]. Recently, a quick homogenous precipitation method was designed to prepare MoS_3 precursors which can produce MoS_2 nanoparticles in various shapes at 780 °C in H_2 [27,28]. The catalytic activity of the as-prepared nano-MoS_2 was also investigated, and the relationship between the catalytic properties and the morphology of MoS_2 was also discussed [29,30].

Based on these facts, nano-MoS_2 reveals a significant advantage over TiO_2, i.e., the band gap of nano-MoS_2 is small enough to allow most of solar light to be absorbed. Previously, the catalytic activ-

* Corresponding author at: Department of Chemical and Materials Engineering, Hefei University, Huangshan Road, Hefei 230022, PR China. Tel.: +86 13966745693.
E-mail addresses: hukunhong@gmail.com, hukunhong@163.com (K.H. Hu).

1385-8947/$ – see front matter © 2010 Elsevier B.V. All rights reserved.
doi:10.1016/j.cej.2010.06.011

ity of MoS_2 nanoclusters obtained by an inverse micelle technique was investigated by Thurston and Wilcoxon et al. [17,31]. A major drawback for this method is that Mo(IV) halides used are not stable compounds. Thus, a modified hydrothermal method was reported to address this problem [32]. Though the hydrothermal method was an effective approach to synthesizing MoS_2 nanoparticles, it was not very convenient because of the need for high-pressure equipment. Moreover, this method did not provide a direct method for obtaining nano-MoS_2/TiO_2 composites. To overcome these disadvantages, the MoS_3/TiO_2 composite was synthesized by a quick deposition of MoS_3 on acid-activated TiO_2. The nano-MoS_2/TiO_2 composite was then prepared by calcining the obtained MoS_3/TiO_2 composite. The resultant nano-MoS_2/TiO_2 composite from this particular route showed a high catalytic activity for the removal of methyl orange from an aqueous solution [33]. The method provides a new approach to synthesize MoS_2 composite catalytic materials. The present work investigated the synthesis of MoS_2/kaolin composite materials by the method. The photocatalytic activity of the as-prepared composite was investigated. The kaolin mineral is very cheap and easily obtained. Thus, using the kaolin mineral to partly replace nano-MoS_2 or TiO_2 is very low-cost and has practical applications.

2. Experiment

2.1. Synthesis of nano-MoS_2/kaolin composite

Kaolin [$Al_2Si_2O_5(OH)_4{\cdot}2H_2O$, chemical grade] was purchased from Sinopharm Chemical Reagent Co. Ltd. $Na_2S{\cdot}9H_2O$, $Na_2MoO_4{\cdot}2H_2O$, HCl, and other reagents were of analytical grade. A typical preparation process is described as follows: 0.6 g $Na_2MoO_4{\cdot}2H_2O$ and 3.4 g $Na_2S{\cdot}9H_2O$ were dissolved in 100 mL de-ionized water. Then, 10 mL alcohol was added into the reaction system. 0.37 g kaolin was dispersed in the obtained solution, and 4.0 mL 12 M HCl was dumped into the reaction system. The resultant precipitation was washed by de-ionized water and dried at 105 °C. The as-synthesized precursor was calcined in a tube furnace at 450 °C for 30 min under a flow of highly pure hydrogen (99.999%). The desired nano-MoS_2/kaolin samples were obtained. A nano-MoS_2 sample without Kaolin was also prepared by a similar method.

2.2. Characterization

Powder X-ray diffraction (XRD) was performed on a Rigaku model D/Max-γB diffractometer with Cu Kα radiation. Micrographs were obtained using a JEOL model 2010 high-resolution transmission electron microscopy (HRTEM) and a Philips model XT30 ESEM-TMP scanning electron microscope (SEM). Thermal analysis was done on a Shimazu model DTG-60H Thermal Analysis Instruments. The Brunauer–Emmett–Teller (BET) surface area was determined using a Micromeritics model ASAP 2020M+C physical and chemical adsorption analyzer. Ultraviolet–visible (UV–vis) light spectral analysis was done on a Shimazu model UV-2550 UV–vis spectrometer. Fourier transform infrared (FTIR) spectra were recorded using a Shimazu model FTIR-8400S IR spectrometer.

2.3. Catalytic experiments

The photocatalytic activities of the obtained composite catalysts were evaluated according to the decoloration rate (%) of the methyl orange solution in a quartz glass reactor. The indoor weak sunlight was selected as environmental lights with a 30 W daylight lamp for illumination. The UV light was weak enough to be neglected, and only the visible light was considered in the indoor environment. To avoid the influence from the instability of the used light, the same serial experiments were done as simultaneously as possible. A typical catalytic experiment is described as follows:

First, 0.2 g nano-MoS_2/kaolin was added into a 150 mL 20 mg/L methyl orange solution at 10 °C, and the obtained suspension was placed in a darkroom and stirred for 15 min to complete the adsorption balance. Then, the catalytic reaction continued under the indoor visible light. About 2 mL of reaction suspension was sucked after every 30 min using an injector. Then, it was clarified by 3000 r/min centrifugation for 5 min. The absorbance (A) of the clarified solution was measured on a 721 spectrophotometer (Shanghai Precision & Scientific Instrument Company, China). The decoloration rate (%) was accounted according to the formula: decoloration rate (%) = $(A_0 - A)/A_0$. After the catalytic reaction, the suspension was filtered. One part of the filtration residue was used for IR characterization and the other for investigating the regeneration of catalyst.

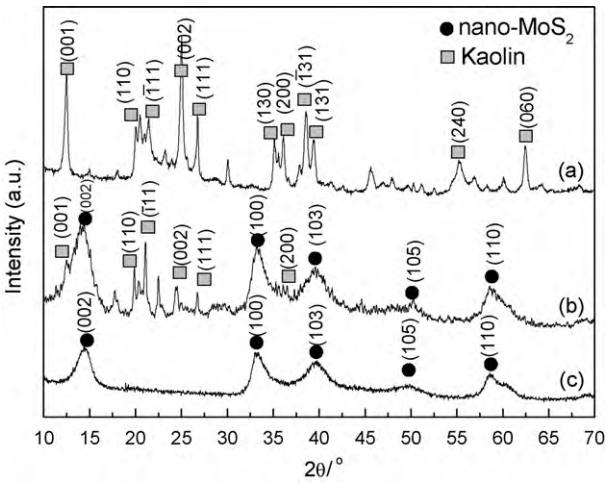

Fig. 1. XRD patterns of samples: (a) kaolin, (b) nano-MoS_2/kaolin and (c) nano-MoS_2.

3. Results and discussion

3.1. Synthesis and characterization of nano-MoS_2/kaolin composite

The nano-MoS_2/kaolin composite [kaolin:MoS_2 (wt:wt) = 1:2, calculated according to the weight change in the obtained precipitation] was fully characterized. The XRD patterns of the nano-MoS_2/kaolin composite are shown in Fig. 1(b), compared with these of pure kaolin and nano-MoS_2 in Fig. 1(a) and (c). The XRD peaks in Fig. 1(a) were indexed to kaolin according to the PDF#89-6538 card. The main diffraction peaks of kaolin were present in the XRD pattern of the nano-MoS_2/kaolin composite in Fig. 1(b). Moreover, the four main diffraction peaks reported in a previous study [28] of nano-MoS_2, i.e., (0 0 2), (1 0 0), (1 0 3), and (1 1 0) also occurred in Fig. 1(b). All the XRD peaks in Fig. 1(b) can be indexed to kaolin and nano-MoS_2, indicating that possible new phases, such as sulfides and oxides, were not formed. The findings confirm that the nano-MoS_2/kaolin composite was successfully prepared. Although the kaolin was not obviously destroyed during the synthesis process, there were still changes in the XRD pattern of the composite compared with that of pure kaolin. The relative intensity of the XRD peaks, especially (0 0 1) and (0 0 2) peaks, concerning kaolin was remarkably weakened in the composite. The X-ray diffraction of (0 0 l) crystal plane was influenced because nano-MoS_2 particles entered into the interlayer space of kaolin, which was confirmed by the SEM images.

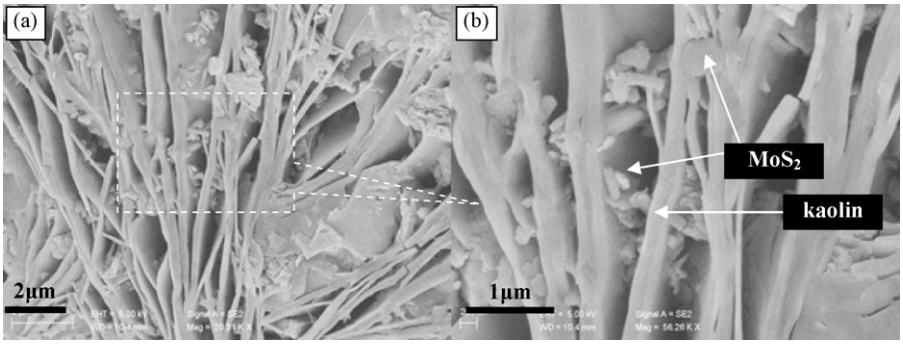

Fig. 2. SEM images of the nano-MoS_2/kaolin composite: (a) typical region and (b) magnified part of (a).

SEM images of the prepared nano-MoS_2/kaolin composite are shown in Fig. 2. The kaolin particles in the figure had a laminated structure, which was composed of many flakes of kaolin. The flakes stacked each other and form a lot of pores, in which the nano-MoS_2 particles lie. The other nano-MoS_2 particles were distributed on the surface of the kaolin.

HRTEM images of the prepared nano-MoS_2/kaolin composite are illustrated in Fig. 3(a) and (b). As shown in the two images, nano-MoS_2 particles with an average length of about 10 nm and an average thickness of about 5 nm were distributed on the surface of kaolin. The size of nano-MoS_2 on the surface of kaolin is smaller than that of both the pure nano-MoS_2 (30–40 nm in length) [28] and the nano-MoS_2 on TiO_2 (10–40 nm in length) [33]. This confirms that the nano-MoS_2/kaolin composite was successfully prepared. The nano-MoS_2 was composed of layered structures containing an interlayer distances of 0.62 nm, corresponding to the interlayer distance of the typical 2H–MoS_2. The typical 2H–MoS_2 layered structure has a 0.615 nm interlayer distance ($2\theta = 14.4^\circ$). The layered structure and lattice parameters of nano-MoS_2 have been discussed using HRTEM, XRD and electron diffraction in Ref. [21].

It is well known that nano-MoS_2 can be prepared according to the following reactions [28]:

$$4S^{2-} + MoO_4^{2-} + 10H^+ \rightarrow MoS_3 \downarrow + H_2S \uparrow + 4H_2O \quad (1)$$

$$MoS_3 + H_2 \overset{\text{heating}}{\longrightarrow} \text{nano-}MoS_2 + H_2S \quad (2)$$

when kaolin was added to the reaction (1), the kaolin is not easily soluble in the cold acid solution. However, there still existed a chemical balance on the inner and external surfaces of the kaolin when high-concentration of strong acid was used. This is because that the kaolin contains –Al–O– bonds (regarded as Al_2O_3), and the reaction was shown as follows:

$$Al_2O_3 + 6H^+ \rightleftarrows 2Al^{3+} + 3H_2O \quad (3)$$

Such reaction led to the activation of the kaolin surface and provided nucleation sites on the surface, where MoS_3 can easily deposit to form a homogenous composite. Thus, reaction (1) mentioned above can be mixed with kaolin to produce the nano-MoS_3/kaolin composite according the following reactions: ((4) and (5))

$$S^{2-} + MoO_4{}^{2-} + 10H^+ + \text{kaolin} \rightarrow MoS_3/\text{kaolin} \downarrow + H_2S \uparrow + 4H_2O \quad (4)$$

A relatively low calcining temperature of 450 °C and a short treatment time of 30 min were applied in this work, and the preparation reaction was shown in (5).

$$MoS_3/\text{kaolin} + H_2 \overset{450\ ^\circ C/30\ \text{min}}{\longrightarrow} \text{nano-}MoS_2/\text{kaolin} + H_2S \quad (5)$$

The reaction (5) was studied by a chemical method: using $CuSO_4$ solution to detect the gas product (H_2S). The blue $CuSO_4$ solution was obviously turned into black CuS by the gas product at ~430 °C, which implies that the preparation of MoS_2/kaolin from MoS_3/kaolin need be treated at >430 °C. A high temperature can increase the crystalline degree of MoS_2. However, it can also lead to the structural changes of the kaolin because of the removal of hydroxyl water and formation of meta-kaolin [34]. This indicates that low temperatures may be better. Taking the heat transfer and temperature distribution of MoS_3/kaolin in the tube furnace into account, the used temperature should be over 430 °C. Therefore, the 450 °C temperature was used in this work. Moreover, long treatment periods can also increase the dehydration of kaolin. The H_2S gas was no longer detected at 450 °C in the reaction (4) after ~20 min, and thus, the 30 min treatment was selected.

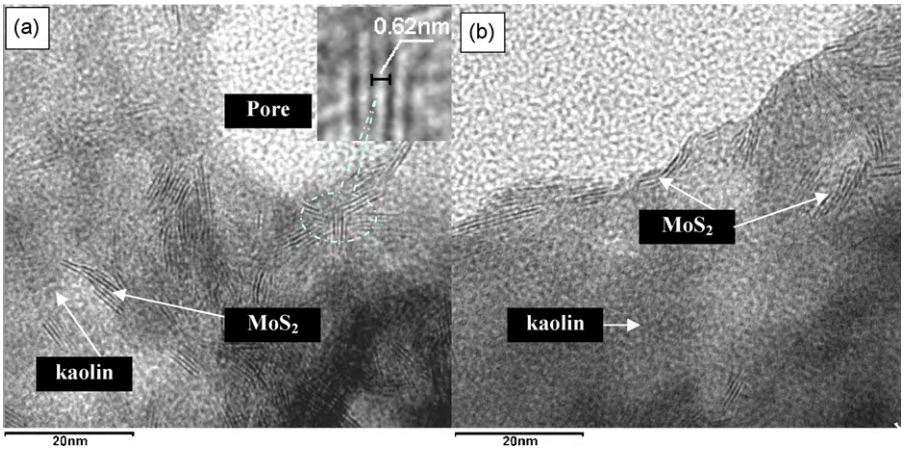

Fig. 3. HRTEM micrographs of the nano-MoS_2/kaolin composite: (a) typical surface in a pore region and (b) typical region of the surface.

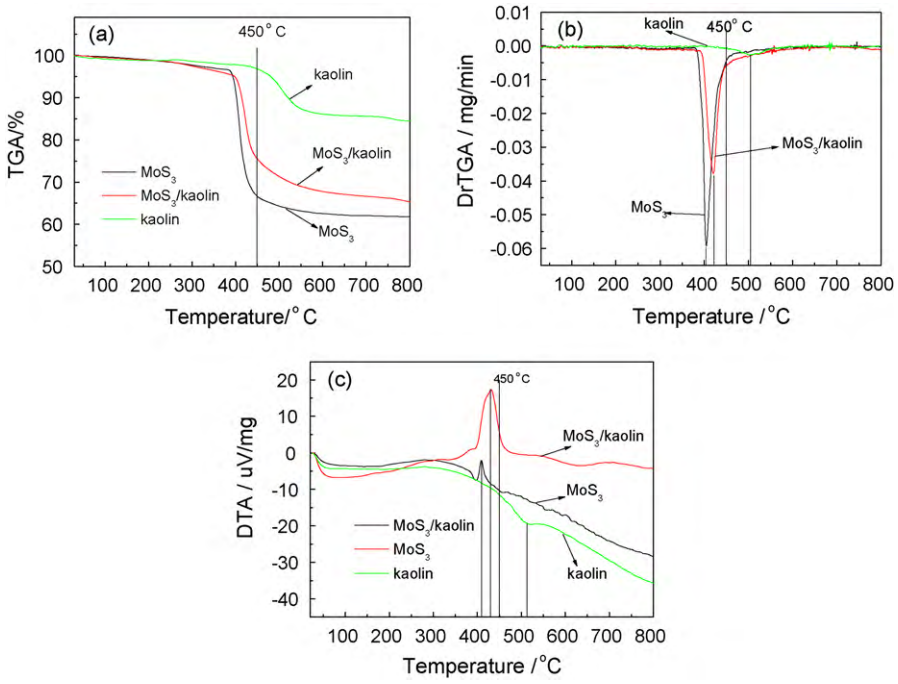

Fig. 4. Thermal analysis of samples: (a) TGA, (b) DrTGA, and (c) DTA.

The discussion mentioned above was confirmed by the thermal analysis results of MoS_3, MoS_3/kaolin, and kaolin, which are provided in Fig. 4, including TGA, DrTGA and DTA of samples. Fig. 4(a) and (b) indicates that the initial decomposition temperature of MoS_3 is at ~390 °C, MoS_3/kaolin at ~400 °C. The peak temperature of MoS_3 decomposition is at ~405 °C, while MoS_3/kaolin at 420 °C, close to the result of the chemical detecting with $CuSO_4$. The removal of hydroxyl water of the pure kaolin begins at ~400 °C, while the obviously dehydration of kaolin can only be observed over 450 °C. When the calcining temperature of 450 °C was used, the MoS_3/kaolin can mostly be turned into MoS_2/kaolin and the kaolin in the composite was slightly affected.

UV–vis light spectra of the prepared nano-MoS_2/kaolin and the pure nano-MoS_2 are shown in Fig. 5. The UV–vis spectrum of the nano-MoS_2/kaolin composite reveals three peaks labeled as (1)–(3) [cf. Fig. 5]. Peak (1) in Fig. 5 can be ascribed to the absorption of nano-MoS_2/kaolin in the UV region. The nano-MoS_2/kaolin composite also has observable absorbance in the visible light region at ~425 nm (380–500 nm). Moreover, there is a very weak peak (3) in the figure. Compared with the UV–vis spectrum of the pure nano-MoS_2, the absorption peaks (2) and (3) of nano-MoS_2/kaolin show large blueshifts. The peak (2) obviously becomes intense, while the peak (3) is weakened.

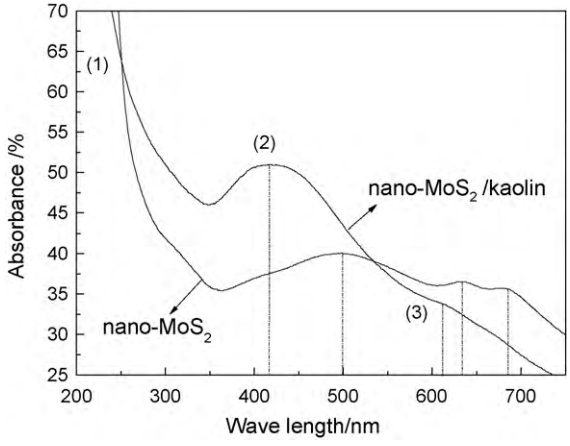

Fig. 5. UV–vis light spectrum of the nano-MoS_2/kaolin composite and pure nano-MoS_2.

The UV–vis absorption behavior of nano-MoS_2 is close relative to its sizes [33,35–38]. Hu et al. reported that the nano-MoS_2/TiO_2 showed two main absorption peaks at ~470 and ~650 nm [33]. The nano-MoS_2/kaolin composite used in the work show a strong absorption at ~425 nm and a very weak one at ~650 nm. Thurston and Wilcoxon reported that the absorption peak of MoS_2 (d = 8–10 nm) was at ~700 nm, while that of MoS_2 (d = 4.5 nm) was at ~470 nm in the visible light region [17]. The nano-MoS_2 in the nano-MoS_2/TiO_2 composite exhibited varying sizes from 2 to 40 nm [33], which led to the appearance of the two absorption peaks reported in Ref. [17]. The thickness of nano-MoS_2 in the nano-MoS_2/kaolin composite is ~5 nm and the peak should occurs in ~470 nm. However, the combination of kaolin and nano-MoS_2 gives rise to a blueshift and the peak shifts to 425 nm. The 425 nm is the lowest allowed transition of MoS_2 and is a mixture of x–y and z polarizations [38].

It was reported that the bulk MoS_2 has absorption edges at 1040 nm (1.23 eV band gap) [35]. The large blueshifts of nano-MoS_2 resulted from its strong quantum confinement effect [7,17,36,37]. The quantum effect also increases the band gap of nano-MoS_2, and its redox potentials are accordingly changed. The appropriate alternation in the energy levels of the conduction and valence band edges allow MoS_2 nanoclusters to act as photocatalysis [14]. A more detailed description about the size-dependent spectroscopy of MoS_2 nanoclusters can be found in [38].

To investigate the influence of the surface area, BET surface areas were measured and are listed in Table 1. The kaolin exhibited

Table 1
BET surface areas of samples.

Sample	Kaolin	Nano-MoS_2/kaolin	Nano-MoS_2
BET surface area (m^2/g)	21	16	31

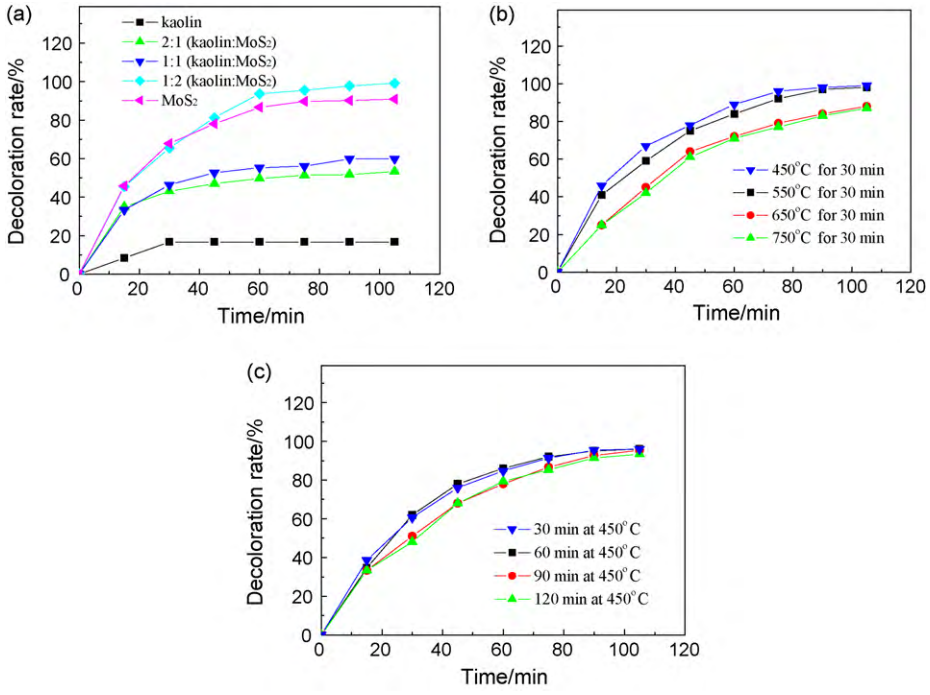

Fig. 6. Influence of the preparation conditions of nano-MoS_2/kaolin composite on the decoloration rate of methyl orange solution: (a) catalyst composition, (b) calcining temperature of MoS_3/kaolin, and (c) calcining time of MoS_3/kaolin.

a relatively high BET surface area (21 m^2/g), and the nano-MoS_2 had the highest BET surface area (31 m^2/g). The surface area of the nano-MoS_2/kaolin composite was decreased to 16 m^2/g when nano-MoS_2 was combined with kaolin. The TGA/DrTGA/DTA results of the composite shows the removal of hydroxyl water of the pure kaolin begins at ~400 °C, and the slight dehydration of kaolin can be observed at 450 °C (see Fig. 4). The decrease in BET surface area resulted from the heating treatment from MoS_3/kaolin to MoS_2/kaolin in H_2 at 450 °C.

3.2. Catalytic activity of MoS_2/kaolin composite

Taking the instability of the indoor and outdoor sunlight into account, the same serial catalytic experiments were done as simultaneously as possible, and the results are shown in Fig. 6. As shown in Fig. 6(a), the catalytic activity increased with the increasing contents of nano-MoS_2 in the composite. The highest decoloration rate (~99%) appeared in the composite with a weight ratio of 1:2 (kaolin:MoS_2). Hu et al reported that the anatase nano-TiO_2 had a very high BET surface area (~227 m^2/g), it still showed a very low activity for degrading methyl orange under indoor visible light [33]. This is because its absorption occurs in the UV region. Though nano-MoS_2 only has a BET surface area of 31 m^2/g, it had an obvious absorption in the visible light region and exhibited a high activity for the degradation of methyl orange. The deposition of nano-MoS_2 on the kaolin particles did not increase the surface area of the nano-MoS_2/kaolin composite. However, the activity of the composite with a weight ratio of 1:2 (kaolin:MoS_2) was better than that of the pure nano-MoS_2. The pure kaolin has no photocatalytic activities and was not an active component in the composite catalyst. It looked as if the kaolin only functioned as the catalyst supporter. However, the use of kaolin has another effect on the nano-MoS_2 based catalysts, i.e. the kaolin can decrease the sizes of nano-MoS_2 and improve the UV–vis absorption of the composite. As has been discussed above, the UV–vis absorption behavior of nano-MoS_2 is close relative to its sizes. The Fig. 3 shows that the composite includes nano-MoS_2 particles with an average length of about 10 nm and an average thickness of about 5 nm on the surface of kaolin. The sizes of the composite are smaller than these (30–40 nm) of nano-MoS_2 with a similar method reported in Ref. [28]. The small sizes of the composite lead to large blueshifts compared with the pure nano-MoS_2, and the blueshift peak (2) at ~425 nm of the nano-MoS_2/kaolin composite obviously becomes more intense than that of the pure nano-MoS_2 (see Fig. 5), Therefore, the nano-MoS_2/kaolin composite showed a high catalytic activity.

Fig. 6(b) and (c) shows that the influence of the calcining temperature and time of MoS_3/kaolin on the catalytic activity of MoS_2/kaolin. Fig. 6(b) indicates that the increasing temperature had a disadvantageous effect on the catalytic activity of the composite catalyst. In addition, the influence of the calcining temperature is insignificant from 450 to 550 °C or from 650 to 750 °C. The degradation curves in Fig. 6(c) indicates that the prolonged calcining time

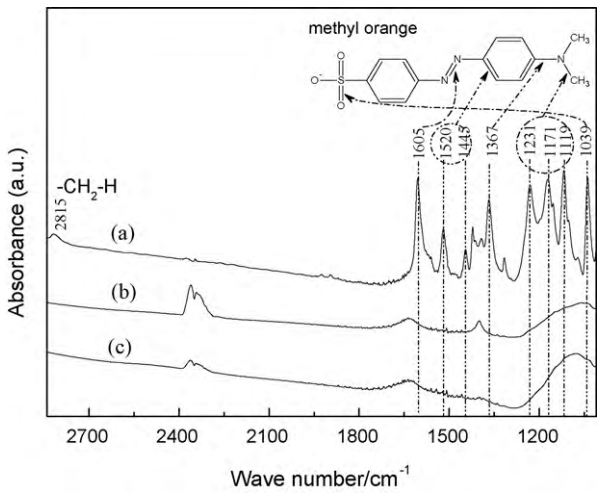

Fig. 7. FTIR spectra of samples: (a) pure methyl orange, (b) nano-MoS_2/kaolin, and (c) nano-MoS_2/kaolin after catalytic degradation of methyl orange.

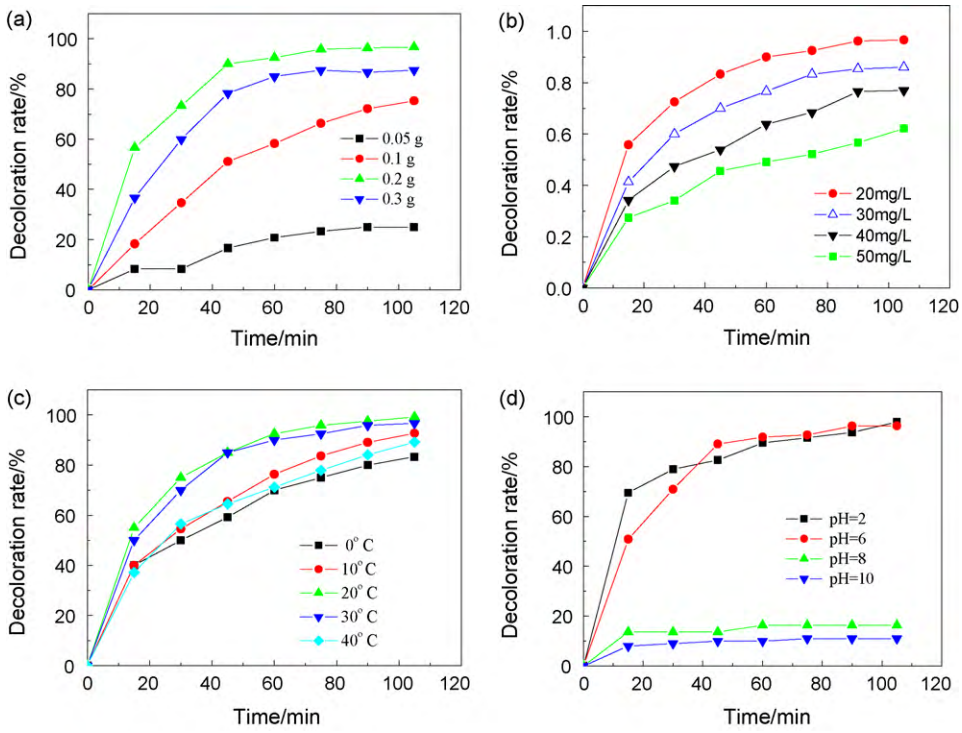

Fig. 8. Effect of conditions on the decoloration rate of methyl orange: (a) nano-MoS_2/kaolin amount, (b) initial concentration of methyl orange, (c) degradation temperature, and (d) initial pH value.

had a weak effect on the catalytic activity of the MoS_2/kaolin composite and slightly decrease the decoloration of methyl orange. The two figures also imply that the selected temperature (450 °C) and time (30 min) in the preparation of MoS_2/kaolin from MoS_3/kaolin is reasonable.

FTIR spectroscopy were used to clarify that the high decoloration rate of methyl orange was not caused by its adsorption on the catalyst, and the results are shown in Fig. 7. Pure methyl orange represented a lot of transmittance peaks at 1000–1700 cm^{-1} [cf. Fig. 7(a)], and the main peaks are marked in this figure. These peaks belong to the functional groups like –N=N–, benzene ring, and –N–C–. The IR spectrum of the nano-MoS_2/kaolin composite after catalytic reaction is shown in Fig. 7(c). It is similar to that of pure nano-MoS_2 [Fig. 7(b)], in which the peaks of methyl orange cannot be found. This finding indicates that the adsorbed methyl orange on the surface of the composite catalyst degraded completely. Therefore, the decoloration of the methyl orange solution was induced by the degradation rather than by the adsorption of methyl orange on nano-MoS_2/kaolin.

It was difficult to clarify the catalytic mechanisms for MoS_2 by designing experiments in this paper, so instead a speculative mechanism that has been proposed in [14,31,39,40] is presented. The photocatalytic activity of the MoS_2 catalyst under visible light was attributed to the formation of surface-adsorbed hydroxyl radicals (·OH) from the adsorbed water by valence band holes [14].

$$MoS_2 \ldots H_2O + h\nu \rightarrow MoS_2 + \cdot OH + H^+ \quad (6)$$

Though the degradation process, with a number of degradation products, is very complex, the degradation mechanism of methyl orange was well studied by Baiocchi et al. [39]. The photoexcited electron was scavenged by the oxygen in the water, finally forming ·OH radicals to degrade the organic chemicals to a lot of intermediates.

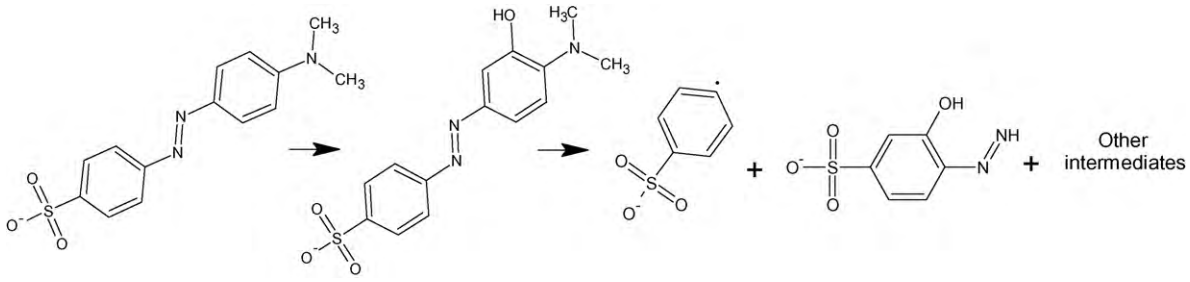

(7)

The total mineralization of methyl orange can be expressed by the following equation, similar to the reaction reported in [40].

$$C_{14}H_{14}N_3SO_3^-(\text{methylorangeion}) + 2H^+ + (31/2)O_2 \rightarrow 3NH_4^+ + SO_4^{2-} + 14CO_2 + 2H_2O \quad (8)$$

3.3. *Effect of degradation conditions*

The influence of the amount of nano-MoS_2/kaolin on the decoloration rate of methyl orange solution is shown in Fig. 8(a). Generally, the catalytic capability can be improved with increasing amounts of the catalyst. In this work, the decoloration rate of the methyl orange solution also increased with increasing contents

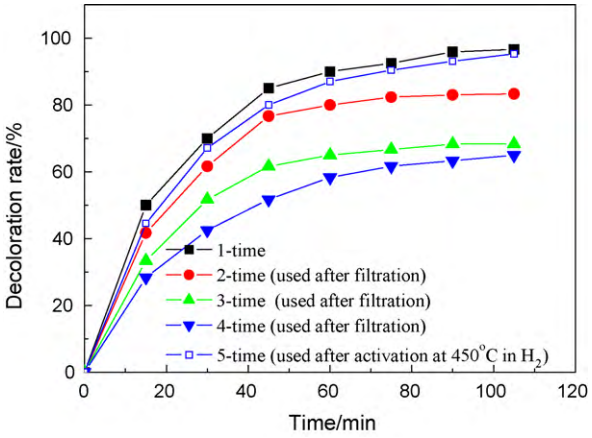

Fig. 9. Influence of the repeated use of the nano-MoS_2/kaolin catalyst on the decoloration rate of the methyl orange solution.

of the catalysts. When the amount of the catalyst was increased to 0.2 g/150 mL methyl orange solution, the decoloration rate within 105 min attained a satisfactory value (~97%). However, when the amount was increased from 0.2 to 0.3 g for 150 mL methyl orange solution (20 mg/L), the decoloration rate decreased a little. This implies that the optimal amount of the composite catalyst was about 0.2 g/150 mL methyl orange under the given reaction conditions. The overmuch amount of MoS_2 blocked the scattering of light in the solution.

The effect of the initial concentration of methyl orange on the decoloration rate is shown in Fig. 8(b). The decoloration rates decreased when the initial concentrations increased. The decoloration was satisfactory only when the initial concentrations were about <40 mg/L. The higher initial concentrations exceeded the treatment capability of the 0.2 g composite catalyst used.

The degradation curves at different temperatures are shown in Fig. 8(c). When 0.2 g catalyst was employed in the 150 mL solution, the decoloration rate at 0–30 °C was relatively high, reaching a peak at 20 °C. However, the decoloration rate began to decrease at 40 °C. The figure also indicates that the temperature had a weaker influence on the photocatalytic rate than other conditions such concentration and pH. The photocatalytic reaction results from the formation of photoelectron and photohole, which is rarely influenced by the environmental temperature. Thus, the temperature generally plays a minor role in the photocatalytic reaction. However, the process of the photocatalytic reaction on the catalyst is consistent with a usual surface reaction, including the molecular diffusion of reactants from solution to surface and of products from surface to solution. A high temperature can accelerate the molecular diffusion, and accordingly the decoloration rate was increased. However, a too high temperature such as 40 °C can increase the evaporation of water to the reactor. The increase in humidity led to a decrease in p_{O_2} and reduced the diffusion of O_2 molecule. The high humidity also hindered the transmission of light from environment to the reaction solution. Thus the decoloration of methyl orange was decreased at 40 °C. These mentioned above were confirmed by the work of Qian et al. [41], in which the effect of temperature, humidity and light intensity on photocatalytic oxidation was investigated. The efficiency of photocatalytic oxidation was the highest at 25 °C under 60–72% humidity, reported in [41].

The initial pH value was one of important parameters in the degradation reaction of methyl orange. The influence of the initial pH values on the decoloration rate of methyl orange solution is shown in Fig. 8(d). The acidic condition of the aqueous solution accelerated the degradation of methyl orange. However, methyl orange exhibited a very low decoloration rate under alkaline conditions. Methyl orange includes two molecular structures, i.e., azo methyl orange under alkaline condition and quinoid methyl orange under acidic condition. The easy degradation of methyl orange under acidic condition indicates that the nano-MoS_2/kaolin catalyst had a higher activity for the degradation of the quinoid methyl orange rather than the azo methyl orange. According the reaction (8) of the speculative mechanism, H^+ is one of reactants and the increase in $[H^+]$ (i.e. the decrease in pH value) can accelerate the degradation reaction and elevate the decoloration rate of methyl orange.

3.4. Regeneration of the nano-MoS_2/kaolin catalyst

The influence of the repeated use of the nano-MoS_2/kaolin catalyst on the decoloration rate of the methyl orange solution is shown in Fig. 9. The nano-MoS_2/kaolin catalysts regenerated via filtration held high catalytic activities after two repeated uses. The activity of the four-time regenerated catalyst was decreased to about 68%. However, the deactivating catalyst could be reactivated via heating at 450 °C in H_2 atmosphere (cf. Fig. 9).

4. Conclusions

A novel large-scale preparation of the nano-MoS_2/kaolin composite is presented. The obtained nano-MoS_2/kaolin composite has a good absorption in the visible light region, which leads to high catalytic activity in methyl orange degradation. The composite catalyst may be regenerated by filtration and reactivated by heating in H_2. The composite is one of the promising photocatalytic materials for the removal of organic chemicals from wastewater, such as organic dyes and phenols. The composite perhaps also has potential applications in the hydrodesulfurization of crude oil and the catalytic oxidation of S^{2-}.

Acknowledgments

This work is supported by the National Natural Science Foundation of China (Grant No. 50905054), the Anhui Provincial Foundation for Excellent Young Talents in University (Grant No. 2010SQRL160), and the Foundation of State Key Laboratory of Solid Lubrication (Grant No. 0907).

References

[1] X.G. Hou, M.D. Huang, X.L. Wu, A.D. Liu, Preparation and studies of photocatalytic silver-loaded TiO_2 films by hybrid sol–gel method, Chem. Eng. J. 146 (2009) 42–48.
[2] S.X. Min, F. Wang, Y.Q. Han, An investigation on synthesis and photocatalytic activity of polyaniline sensitized nanocrystalline TiO_2 composite, J. Mater. Sci. 42 (2007) 9966–9972.
[3] X. Cao, Y. Oda, F. Shiraishi, Photocatalytic and adsorptive treatment of 2,4-dinitrophenol using a TiO_2 film covering activated carbon surface, Chem. Eng. J. 156 (2010) 98–105.
[4] C.C. Chan, C.C. Chang, W.C. Hsu, S.K. Wang, J. Lin, Photocatalytic activities of Pd-loaded mesoporous TiO_2 thin films, Chem. Eng. J. 152 (2009) 492–497.
[5] B.M. Reddy, G.K. Reddy, K.N. Rao, I. Ganesh, J.M.F. Ferreira, Characterization and photocatalytic activity of TiO_2–M_xO_y (M_xO_y = SiO_2, Al_2O_3, and ZrO_2) mixed oxides synthesized by microwave-induced solution combustion technique, J. Mater. Sci. 44 (2009) 4874–4882.
[6] B.T. Jiang, S.Y. Zhang, X.Z. Guo, B.K. Jin, Y.P. Tian, Preparation and photocatalytic activity of CeO_2/TiO_2 interface composite film, Appl. Surf. Sci. 255 (2009) 5975–5978.
[7] J.P. Wilcoxon, P.P. Newcomer, G.A. Samara, Synthesis and optical properties of MoS_2 and isomorphous nanoclusters in the quantum confinement regime, J. Appl. Phys. 81 (1997) 7934–7944.
[8] V. Iliev, L. Prahov, L. Bilyarska, H. Fischer, G. Schulz-Ekloff, D. Wöhrle, L. Petrov, Oxidation and photooxidation of sulfide and thiosulfate ions catalyzed by transition metal chalcogenides and phthalocyanine complexes, J. Mol. Catal. A: Chem. 151 (2000) 161–169.
[9] E. Benavente, M.A. Santa Ana, F. Mendizábal, G. González, Intercalation chemistry of molybdenum disulfide, Coord. Chem. Rev. 224 (2002) 87–109.

[10] J. Valyon, W.K. Hall, The chemisorption of O_2 and NO on reduced and sulfided molybdena-alumina catalysts, J. Catal. 84 (1983) 216–228.
[11] J.T. Richardson, Electronic properties of unsupported cobalt-promoted molybdenum sulfide, J. Catal. 112 (1988) 313–319.
[12] W.S. Millman, K. Segawa, D. Smrz, W.K. Hall, A comparison of the surface chemistry and catalytic properties of reduced vs sulfided molybdena-alumina catalysts, Polyhedron 5 (1986) 169–177.
[13] S.C. Ray, M.K. Karanjai, D. Gupta, Tin dioxide based transparent semiconducting films deposited by the dip-coating technique, Surf. Coat. Technol. 102 (1998) 73–80.
[14] W.K. Ho, J.C. Yu, J. Lin, J.G. Yu, P.S. Li, Preparation and photocatalytic behavior of MoS_2 and WS_2 nanocluster sensitized TiO_2, Langmuir 20 (2004) 5865–5869.
[15] R. Coehoorn, C. Haas, R.A. de Groot, Electronic structure of $MoSe_2$, MoS_2, and WSe_2. II. The nature of the optical band gaps, Phys. Rev. B 35 (1987) 6203–6206.
[16] E. Pelizzetti, M. Visca, Energy resources through photochemistry and catalysis, in: M. Gratzel, (Ed.), Academic Press, NewYork, 1983, 261.
[17] T.R. Thurston, J.P. Wilcoxon, Photooxidation of organic chemicals catalyzed by nanoscale MoS_2, J. Phys. Chem. B 103 (1999) 11–17.
[18] Y.Y. Peng, Z.Y. Meng, C. Zhong, J. Lu, Z.P. Yang, Y.T. Qian, Tube- and ball-like amorphous MoS_2 prepared by a solvothermal method, Mater. Chem. Phys. 73 (2002) 327–329.
[19] J.H. Zhan, Z.D. Zhang, X.F. Qian, C. Wang, Y. Xie, Y.T. Qian, Solvothermal synthesis of nanocrystalline MoS_2 from MoO_3 and elemental sulfur, J. Solid. State. Chem. 141 (1998) 270–273.
[20] W.J. Li, E.W. Shi, J.M. Ko, Z.Z. Chen, H. Ogino, T. Fukuda, Hydrothermal synthesis of MoS_2 nanowires, J. Cryst. Growth 250 (2003) 418–422.
[21] X.L. Li, Y.D. Li, MoS_2 nanostructures: synthesis and electrochemical Mg^{2+} intercalation, J. Phys. Chem. B 108 (2004) 13893–13900.
[22] P. Afanasiev, G.F. Xia, G. Berhault, B. Jouguet, Surfactant-assisted synthesis of highly dispersed molybdenum sulfide, Chem. Mater. 11 (1999) 3216–3219.
[23] Y. Feldman, E. Wasserman, D.J. Srolovitz, R. Tenne, High rate, gas phase growth of MoS_2 nested inorganic fullerenes and nanotubes, Science 267 (1995) 222–225.
[24] M.P Zach, K. Inazu, K.H. Ng, J.C. Hemmingr, R.M. Penner, Synthesis of molybdenum nanowires with millimeter-scale length using electrochemical step edge decoration, Chem. Mater. 14 (2002) 3206–3216.
[25] M. Nath, A. Govindaraj, C.N.R. Rao, Simple synthesis of MoS_2 and WS_2 nanotubes, Adv. Mater. 13 (2001) 283–286.
[26] T.Z. Zou, J.P. Tu, H.D. Huang, D.M. Lai, L.L. Zhang, D.N. He, Preparation and tribological properties of inorganic fullerene-like MoS_2, Adv. Eng. Mater. 8 (2006) 289–293.
[27] K.H. Hu, Y.R. Wang, X.G. Hu, H.Z. Wo, Preparation and characterisation of ball-like MoS_2 nanoparticles, Mater. Sci. Technol. 23 (2007) 242–246.
[28] K.H. Hu, X.G. Hu, Formation, exfoliation and restacking of MoS_2 nanostructures, Mater. Sci. Technol. 25 (2009) 407–414.
[29] K.H. Hu, X.G. Hu, Y.F. Xu, X.Z. Pan, The effect of morphology and size on the photocatalytic properties of MoS_2, Reac. Kinet. Mech. Cat. 100 (2010) 153–163.
[30] K.H. Hu, X.G. Hu, X.J. Sun, Morphological effect of MoS_2 nanoparticles on catalytic oxidation and vacuum lubrication, Appl. Surf. Sci. 256 (2010) 2517–2523.
[31] J.P. Wilcoxon, T.R. Thurston, J.E. Martin, Applications of metal and semiconductor nanoclusters as thermal and photo-catalysts, Nanostruct. Mater. 12 (1999) 993–997.
[32] B. Pourabbas, B. Jamshidi, Preparation of MoS_2 nanoparticles by a modified hydrothermal method and the photo-catalytic activity of MoS_2/TiO_2 hybrids in photo-oxidation of phenol, Chem. Eng. J. 138 (2008) 55–62.
[33] K.H. Hu, X.G. Hu, Y.F. Xu, J.D. Sun, Synthesis of nano-MoS_2/TiO_2 composite and its catalytic degradation effect on methyl orange, J. Mater. Sci. 45 (2010) 2640–2648.
[34] F. Gao, Z.L. Zhao, H. Cui, J.Y. Zhang, B.J. Zhang, DTA characteristics of coal series kaolinite, J. Fuel Chem. Technol. 26 (1998) 24–29 (in Chinese).
[35] K.K. Kam, B.A. Parkinson, Detailed photocurrent spectroscopy of the semiconducting group VIB transition metal dichalcogenides, J. Phys. Chem. 86 (1982) 463–467.
[36] J.M. Huang, R.A. Laitinen, D.F. Kelley, Spectroscopy and trapping dynamics in WS_2 nanoclusters, Phys. Rev. B 62 (2000) 10995–11005.
[37] J.P. Wilcoxon, Catalytic photooxidation of pentachlorophenol using semiconductor nanoclusters, J. Phys. Chem. B 104 (2000) 7334–7343.
[38] V. Chikan, D.F. Kelley, Size-dependent spectroscopy of MoS_2 nanoclusters, J. Phys. Chem. B 106 (2002) 3794–3804.
[39] C. Baiocchi, M.C. Brussino, E. Pramauro, A.B. Prevot, L. Palmisano, G. Marcì, Characterization of methyl orange and its photocatalytic degradation products by HPLC/UV–VIS diode array and atmospheric pressure ionization quadrupole ion trap mass spectrometry, Int. J. Mass. Spectrom. 214 (2002) 247–256.
[40] M. Tamimi, S. Qourzal, A. Assabbane, J.-M. Chovelon, C. Ferronatob, Y. Ait-Ichou, Photocatalytic degradation of pesticide methomyl: determination of the reaction pathway and identification of intermediate products, Photochem. Photobiol. Sci. 5 (2006) 477–482.
[41] C.X. Qian, L.F. Zhao, D.F. Fu, L. Li, R.X. Wang, Study on the effect of temperature, humidity and light intensity on photocatalytic oxidation of NO_2 by nano-TiO_2 immobilized on cement-based materials, Acta Scientiae Circumstantiae 25 (2005) 623–630.